Vortex kinematic around a submerged plate under water waves. Part I: Experimental analysis

Adrien Poupardin, G. Pérret, G. Pinon, Nicolas Bourneton, Elie Rivoalen, Jérôme Brossard

Vortex kinematic around a submerged plate under water waves. Part I: Experimental analysis

Adrien Poupardin, G. Pérret, G. Pinon, Nicolas Bourneton, Elie Rivoalen, Jérôme Brossard

Vortex kinematic around a submerged plate under water waves. Part I: Experimental analysis

A. Poupardin [a], G. Perret [a,*], G. Pinon [a], N. Bourneton [b], E. Rivoalen [c], J. Brossard [a]

[a] Laboratoire Ondes et Milieux Complexes (LOMC), UMR 6294, CNRS-Université du Havre, 53, rue de Prony, BP540, 76058 Le Havre Cedex, France
[b] CETE, CETMEF, rue Viviani, BP 46223 Nantes Cedex 2, France
[c] Laboratoire d'Optimisation et Fiabilité en Mécanique des Structures (LOFIMS), EA 3828, INSA de Rouen, Avenue de l'Université, BP 08, 76801 Saint Etienne du Rouvray, France

ARTICLE INFO

Article history:
Received 31 July 2011
Received in revised form
13 February 2012
Accepted 14 February 2012
Available online 20 February 2012

Keywords:
Vortex dynamics
Submerged plate
Water waves

ABSTRACT

This paper presents the vortex dynamics generated by the interaction of a submerged horizontal plate, considered as a vortex generator, and a monochromatic wave. The velocity and vorticity fields are determined experimentally using PIV technique for different resolutions in order to study the global flow around the plate and the formation and advection of vortices upstream and downstream of the plate. The global flow around the plate shows great discrepancies with the potential flow solution: two recirculation cells are formed beneath the plate, the global flow is non-symmetric and the advection of vortices induces strong velocities not represented by the potential flow theory. The formation of vortices at the edges of the plate is characterised. At each period, one vortex is formed at the edge followed by the formation of an opposite sign vortex. The upstream and downstream vortex pairs are then advected in front of the plate and toward the bottom respectively, over a distance of about one third the plate length. The lifetime of vortices is about two wave periods. This study will help us validate a numerical software to be used for analysing the influence of various parameters on the dynamics. These results will be presented in the second part of this paper.

1. Introduction

The new requirements in terms of environmental impact of coastal structures and the emergence of marine energy converters compel designers to gain a better understanding of the flow field around marine structures. The interaction of waves and currents with submerged structures, such as offshore structures, coastal protection breakwaters or wave and current energy converters, generate small-scale hydrodynamic phenomena which cannot be neglected by civil engineers. Indeed, the development of boundary layers at the obstacle surfaces and flow separations at angular corners or edges lead to the generation and shedding of vortices. Such vortices may have various consequences such as dissipation, interaction with the free surface, the bottom or other structures, or efforts on structures.

Indeed, vortices lead to energy dissipation through energy cascade from large-scale turbulent eddies to small-scale viscous dissipation [1]. Chang et al. [2] show, for a submerged rectangular obstacle under a solitary wave, that the energy dissipation can reach 15% of the incoming wave energy. However, if diffusion and dissipation are weak enough, vortices can interact with the bottom and the free surface leading to perturbations and even breakup [3]. In the case of sedimentary seabed, vortex/bottom interactions lead to scouring phenomena with two consequences: an increase of turbidity with an impact on marine life and a weakening of marine structure foundations [4,5]. Moreover, the shedding of vortices is the sign that forces are being applied to the immersed structure. Finally, vortices may interact with neighbouring devices in the case of structures arranged in a more or less regular grid, like energy converter farms. Hydrodynamic disturbances induced by these vortices can be detrimental for these devices, modifying their functional behaviour and increasing the hydrodynamic loading forces.

However, despite vortex dynamics surrounding coastal marine structures is of prime interest, this topic has only been studied quite recently, mainly for a submerged dike. Ting and King [6] were among the first to study the kinematics and dynamics of eddy motions in the vicinity of a submerged rectangular obstacle. The measured flow fields exhibit the generation of clockwise and counter-clockwise vortices on either side of the obstacle when time-periodic waves propagate over it. The authors noticed that the flow field is only modified in the vicinity of the obstacles in comparison with linear inviscid theory. Consequently, vortices have little effect on the reflection process. However they also noticed that a major effect of these vortices is to dissipate

* Corresponding author.
E-mail address: perretg@univ-lehavre.fr (G. Perret).

energy. But the lack of accuracy for the energy balance deduced from their data did not allow a precise quantification of the dissipation process. Chang et al. [7] obtained similar results with cnoidal waves propagating over a similar structure, by means of PIV measurements and RANS numerical method. However the modelling techniques used in their study led to a more accurate flow field around the obstacles and allowed a better description of the kinematics. Thus, the interactions between the clockwise and counter-clockwise eddies could be observed more clearly. Their results showed that the vortices were confined within a region of about two or three times the unperturbed wave particle trajectory. A very interesting discussion was presented about the characteristic velocity to choose for vortex intensity scaling. They showed that vortex dynamics was weakly correlated to incident wave characteristics: the usual characteristic scales used to treat the reflection–transmission process under propagating wave conditions could not be maintained.

However, submerged plates can also be used for coastal protection purposes and present some interest in comparison with submerged dikes. Such a system preserves the continuity of the marine environment and leads to more economic design, especially for deep water areas. Nevertheless, the hydrodynamic behaviour of these structures is rather different from a submerged obstacle laid on the sea bed and has been mainly investigated using potential flow theories [8–14]. Based on these theories, Graw [15,16], Carter [17] and Orer and Ozdamar [18] suggested using a submerged plate as an energy converter following experimental observations of a pulsating flow at one location beneath the plate. Lengricht et al. [19] showed, by means of PIV measurements, the generation of a strong vortex at the lee-side of the plate but no description of the kinematics of the vortices was given. Many wave energy converters also use vertical moving flaps systems such as the Oyster system [20–22]. Vortices generated by such systems fixed to the sea bottom, might generate even more important scouring as they are close to the sedimentary bed.

The purpose of the experimental work presented in this first part is to characterise the flow field around the plate and to bring to the fore the role played by vortex shedding and kinematics on the dynamics. Section 2 details the experimental set-up and parameters. Section 3 is devoted to the description of the mean flow around the plate and Section 4 to the vortex dynamics itself. Conclusions are made in Section 5.

In the second part of this study, experimental results will be compared with numerical simulations using a Lagrangian particle method in order to validate the software. This method can describe an unsteady flow field without meshing of the flow domain. The software is based on a potential flow theory and vortices are generated using the Kutta–Joukovsky condition at the edges of the plate [23,24]. Along with the velocity–vorticity formulation of the method (vortex method), this leads to an accurate description of the vortex dynamics close to a thin submerged plate. The numerical model will then be used to identify the key parameters which control the vortex dynamics.

2. Experimental setup

The experiments were performed in a 10 m long, 0.30 m wide and 0.30 m high wave flume (see Fig. 1). The horizontal thin plate was $L = 0.25$ m long, $l = 0.30$ m wide and $e = 0.003$ m thick. It was made of glass to avoid the plate creating a shadow in the laser sheet for the measurement of the whole flow field around the plate. The displacement of the plate due to the wave action was estimated by the measurement of the downstream edge displacement on the zoom visualisation (described below). The maximum displacement observed was $0.0183\,\text{cm} \pm 9 \cdot 10^{-4}$ where the uncertainty was due to the pixel resolution. The wave maker was an oscillating paddle which did not absorb the wave reflected by the plate. Therefore, the incident wave was a monochromatic wave resulting in fact from the multiple reflections between the plate and the wave maker. The incident and reflected waves were discriminated by the Goda–Suzuky method [25] using two probes. A sloping beach at the end of the flume limited the wave reflection to 5%.

In order to focus on vortex dynamics, one wave condition was chosen such that the production of harmonics was weak (Brossard et al. [26]) and the effect of the plate on the free surface was limited. Thus, the incident wave frequency was $f_0 = 1$ Hz, the wave amplitude $a = 0.01$ m and the water depth at rest was $h_0 = 0.20$ m. The flat plate was immersed at $i = 0.07$ m from the free surface. The incident wavelength was thus $\lambda_0 \simeq 1.2$ m according to the dispersion relation (given by first and second order Stokes theory) $f_0 = \sqrt{g/(2\pi\lambda_0)\,\tanh((2\pi\,h_0)/\lambda_0)}$. In this configuration the reflection coefficient induced by the plate was about 25% [26].

Vortex formation and intensity were closely related to the dynamics around the plate. With a plate length $L = 0.25$ m and an incident wavelength $\lambda_0 \simeq 1.2$ m, the presence of the plate strongly influenced the mean flow dynamics (see Section 3). However, to compare the perturbed hydrodynamics to the incident flow conditions, the characteristic velocity scale is defined as the amplitude of the first order Stokes velocity at the immersion depth i:

$$U = a\frac{g}{f_0\lambda_0}\frac{\cosh[2\pi(h_0 - i)/\lambda_0]}{\cosh(2\pi h_0/\lambda_0)} = 0.063\ \text{m s}^{-1}. \quad (1)$$

Compared to Chang et al. [7], who used the mean flow rate over the obstacle, the expression (1) is more realistic in the present case since the flow is allowed under the immersed plate. However, to conclude on the best characteristic velocity for non-dimensionalisation, a complete study of the flow behaviour under wide variations of parameters is required.

The characteristic vorticity is thus $\omega_{\text{ref}} = U/\delta = 111.7\ \text{rad s}^{-1}$, with $\delta = \sqrt{\nu/(\pi f_0)} = 5.64 \cdot 10^{-4}$ m being the boundary layer thickness of a periodic oscillating flow at frequency f_0 [27] and $\nu = 1.10^{-6}\,\text{m}^2\,\text{s}^{-1}$ the kinematic viscosity. The characteristic horizontal and vertical length scales are the half plate length $L/2 = 0.125$ m and the characteristic time scale is the incident wave period $T = 1/f_0 = 1.0$ s. In such conditions, the Reynolds number based on the immersion is $\text{Re} = \frac{Ui}{\nu} = 4415$ and the Keulegan–Carpenter number is $\text{KC} = \frac{TU}{i} = 0.9$.

The Particle Image Velocimetry (PIV) technique was used for the visualisation purpose of the present study. The flow was seeded with spherical polyamid particles of diameter 20 μm and density $1.1\ \text{g cm}^{-3}$. The visualisation zone was lit with a 120 mJ YAG laser, which gave out two light flashes at intervals varying between 0.5 and 7 ms, depending on the resolution, with a frequency of 15 Hz. The particles' motion was recorded with a 1600×1200 pixels CCD camera. To study the flow around the plate, five visualisation zones were defined (Fig. 2): a global zone of 47.7×23 cm including the whole submerged plate, the bottom and the free surface, with a resolution of 33.2 pixels/cm; two zones zoomed on the regions upstream and downstream of the plate with the dimensions 15.1×18.1 cm and 21.7×16.1 cm, and a resolution of 65 pixels/cm and 73 pixels/cm respectively. Two higher zoomed zones were realised on the lee-side edge of the plate with a resolution of 555 pixels/cm in order to study the vortex formation process more precisely.

For each visualisation zone, 50 phases evenly distributed over one period (T) were recorded for 300 periods so that a total of 15 000 instantaneous fields have been recorded for each visualisation zone. For each of the 50 phases, the mean velocity and vorticity fields were obtained, averaging over the 300 instantaneous fields (see Section 3). The obtained velocity field resolutions were 1.43 vectors/cm for the global view,

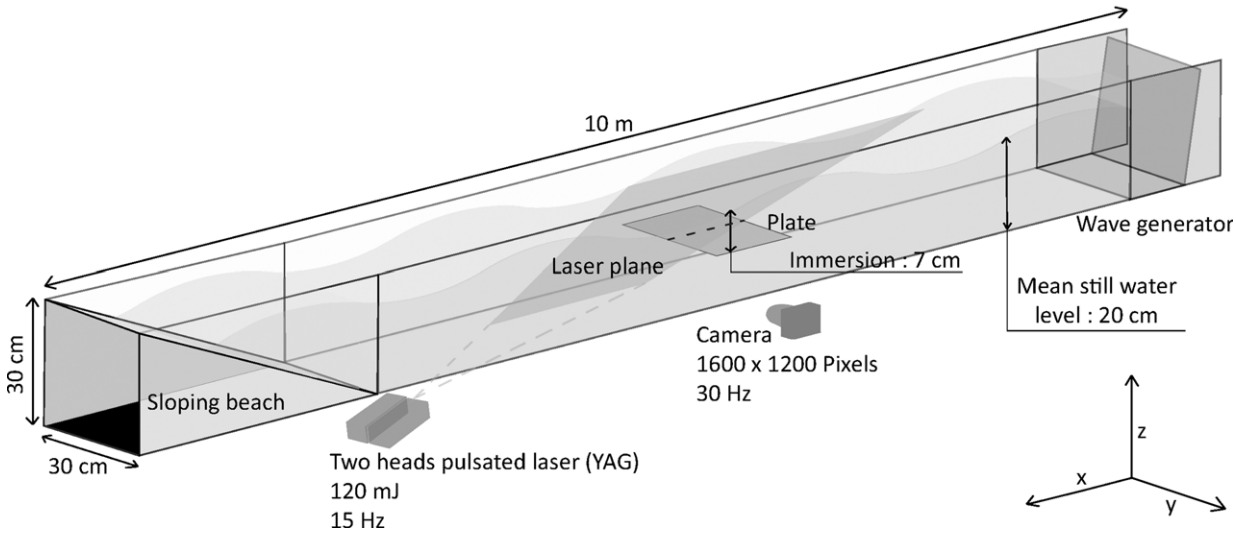

Fig. 1. Experimental scheme of the wave flume.

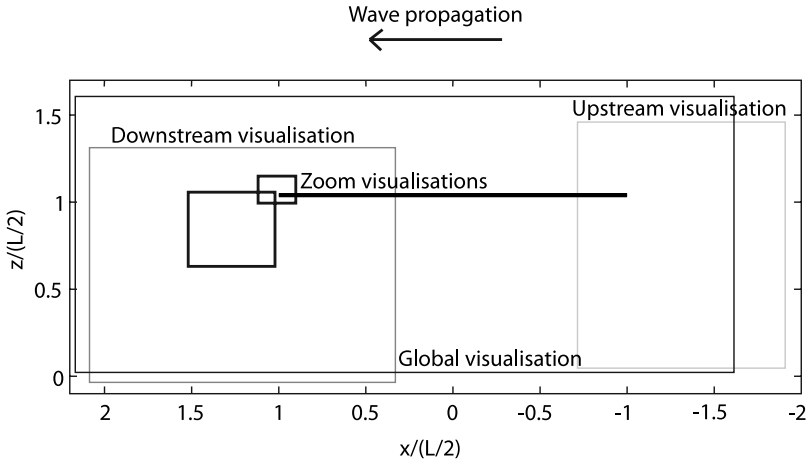

Fig. 2. Scheme of the different visualisations zones.

3.33 vectors/cm for the downstream view, 2.78 vectors/cm for the upstream view and 22.9 vectors/cm for the high zoom views. The vortex core mean position was localised for each of the 50 phases from the mean vorticity fields (see Section 4). Standard deviation was also evaluated over the 300 periods.

The location of the vortices may be precisely determined from experimental velocity or vorticity fields, thanks to several methods [28–31]. Chong et al. [29] studied the eigenvalues of the velocity gradient tensor ∇u. If this tensor has complex eigenvalues, it means that the local streamline pattern is closed or spiral in a reference frame moving with the point. It then corresponds to a vortex core. Hunt et al. [28] suggested that the vortex centre was the point where the antisymmetric part of ∇u is superior to its symmetric part. But this definition does not necessarily define a region with a pressure minimum. Jeong and Hussain [30] developed a method to identify a local pressure minimum and to associate this region to the vortex core. These pressure minima correspond to negative eigenvalues of the velocity gradient tensor. Graftieaux et al. [31] developed another method: a function Γ associates a value at each point of the flow and this value depends on the motion of the fluid. If the flow is rotating around a point, the function Γ is maximised and a vortex core is detected.

All these methods were tested using our velocity and vorticity fields. The most effective was found to be the one developed by Jeong and Hussain [30] called $\lambda 2$ factor. In fact, this method made it possible to locate a vortex core even inside a vortex sheet, whereas a method based on the vorticity maximum failed. Moreover, as opposed to other methods, this one associates a local pressure minimum to a vortex core. Thus, in the next sections, the vortex centre positions were determined with the $\lambda 2$ factor criteria.

3. Mean global velocity field

In order to determine the accumulated effect of the vortices in the vicinity of the plate, the total mean velocity field (Fig. 3) was obtained as the average of the mean velocity fields of the 50 phases, each computed from the 300 periods; *i.e.* an average over all the 15 000 instantaneous fields.

One striking observation is that this total mean flow is non zero over one period and not even symmetric. Two important recirculation cells persist upstream and downstream of the plate (indicated by letters A and B on Fig. 3), which generate strong velocities. In particular, in the lee-side zone, the recirculation cell is associated with a strong vertical jet plunging toward the flume bottom (letter C). This jet impacts the bottom (letter D) at an average distance of about 1/5 of the plate length from the lee-side edge. The location of the stagnation point periodically varies over one wave period with an amplitude of 0.022 m ($\approx 0.09 \times L$). Hence, this stagnation point is highly localised and may lead to important scouring phenomena of the sedimentary seabed in

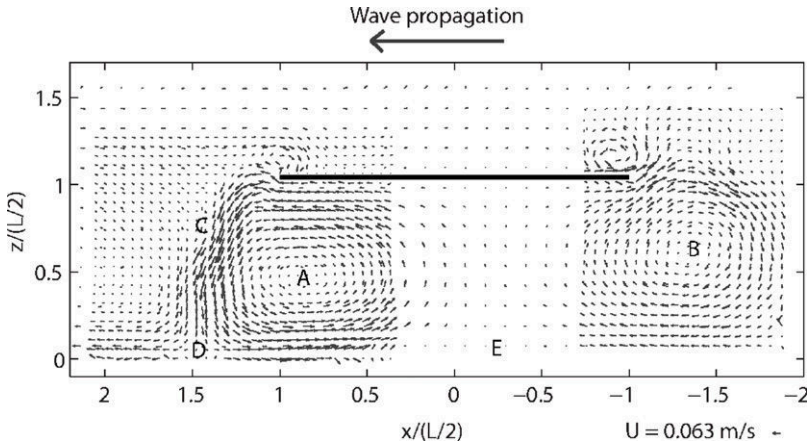

Fig. 3. Mean velocity fields for the five vision zones.

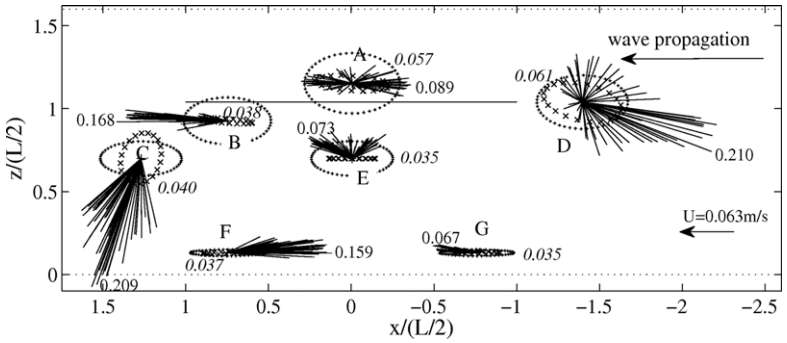

Fig. 4. Measured velocities (straight lines), potential analytical velocities (crosses ×) and undisturbed flow Stokes velocities (points +) given at different locations of the flow over one wave period. The numbers indicate the maximum potential analytical (italic) and measured velocity (normal) values at each point in m s^{-1}.

natural conditions. Another stagnation point (letter E) is located under the plate between the two recirculation cells. The mean position of this second stagnation point is located at a distance equal to 0.36 × *L*, *i.e.* about 1/3 of the plate length, from the upstream edge. However, the position of this stagnation point varies considerably during a wave cycle, from the centre of the plate to approximately 0.14 × *L* downstream during the first half period and to approximately 0.47 × *L* upstream during the second half period. Therefore, the shear stress induced by the flow may strongly modify the seabed morphology. But due to the great variation in the position of the stagnation point, an accumulation of sediments at a specific location under the plate is not to be expected.

The observed flow is very different from the one predicted by potential theory [8,10,12]. To illustrate this difference, the hodographs of the measured and potential analytical velocities at seven fixed locations of the flow have been plotted in Fig. 4 for the 50 phases. Measured velocities (lines) are compared with analytical solutions for a potential flow around a submerged plate (×), based on the theories developed by Takano [8], Massel [10] and Rey et al. [12], and the first order Stokes theory without obstacle (+). The length of the segment is proportional to the velocity value at each phase.

The potential theory shows that the presence of the plate modifies the classical results of Stokes trajectories. Under the plate (points E, F and G), the fluid particles are periodically displaced horizontally from upstream to downstream. At the upstream edge of the plate (point D), the velocities describe a flattened ellipse, orientated slightly toward the bottom. Downstream the plate (point C), the ellipse is more flattened and orientated strongly toward the bottom. However, for all the points, the particles undergo zero mean velocities over one period.

The present measurements show great discrepancies with the theoretical results beneath the plate, and particularly upstream and downstream in zones of strong vortical flows. Under the plate (point E), fluid particles are displaced from right to left but always upward. Close to the bottom (points F and G) velocities are not oscillating anymore but they are orientated in one privileged direction, either toward the weather side (point F) or the lee-side (point G). Downstream of the plate (point C) the flow is only directed toward the bottom during the whole period with very strong velocities of up to 3.3 times the characteristic velocity *U*. As for point D, upstream of the plate, the mean velocity is no longer zero over one wave period and instantaneous velocities are much stronger in the upstream direction. For these two points (C and D), the strong velocities are generated by the induction of two counter rotating vortices. Since the potential analytical theory is inviscid, no vorticity is generated due to boundary and shear layers. Moreover, no point vortices are introduced in the analytical model used here, so that the vortex dynamics is not taken into account. Therefore, the strong discrepancies observed between analytical and experimental results are mainly due to the dynamics of these vortices, *i.e.* their formation, advection and dissipation through energy cascade. Hence, the full vortex dynamics has to be correctly characterised to understand the complex perturbed flow around the plate. This is the object of the following section.

4. Vortex dynamics

The vortices are formed at the plate edges. Fig. 5 depicts vorticity maps of the flow at the lee-side edge, obtained from measurements performed in the zoom visualisation zone, for 8 different phases over one wave period. Fig. 6 depicts unzoomed lee-side (left) and weather side (right) views of the

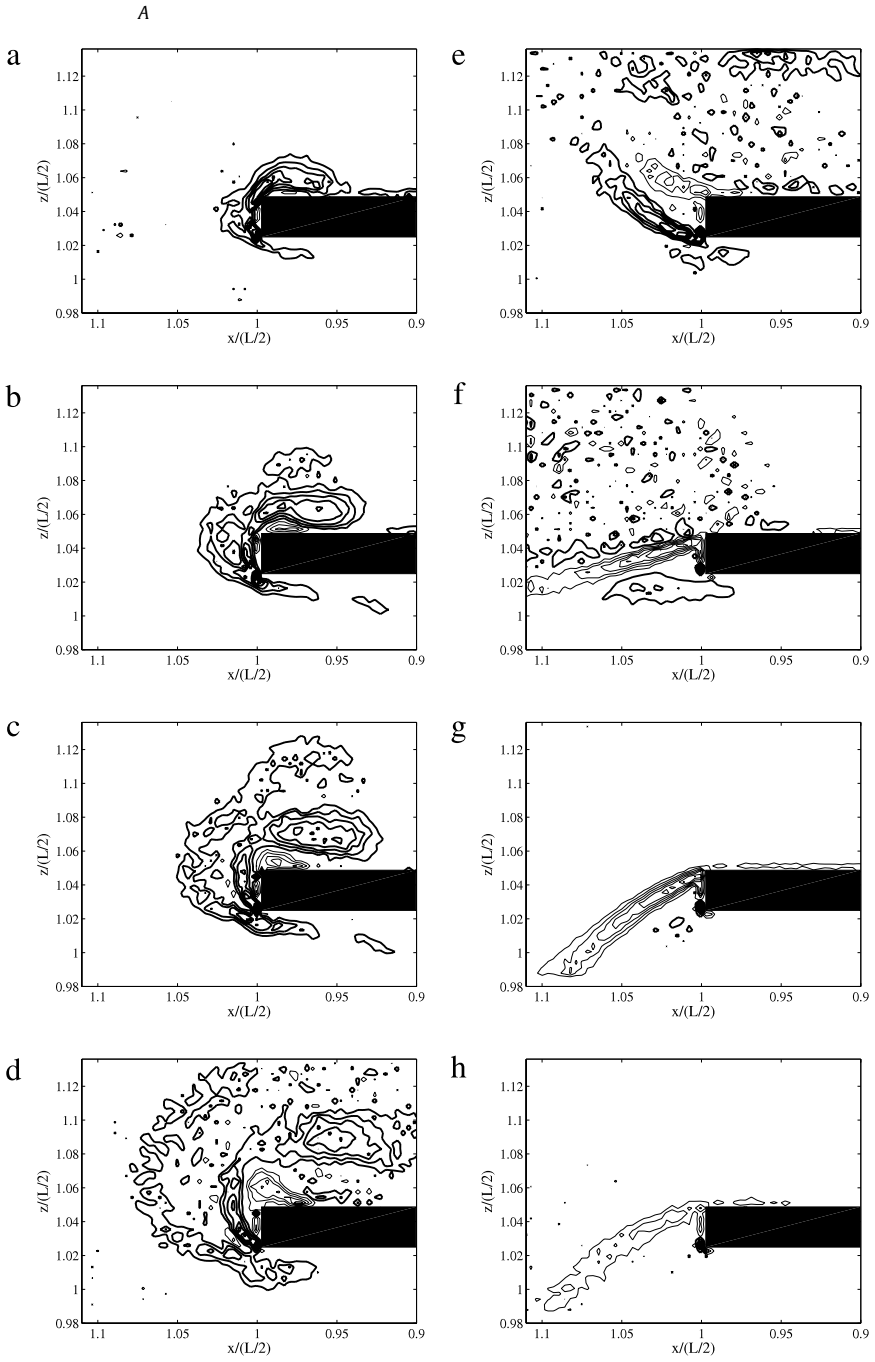

Fig. 5. Mean vorticity fields at the downstream edge of the plate at $t/T = 0$ (a), 0.04 (b), 0.08 (c), 0.16 (d), 0.32 (e), 0.48 (f), 0.68 (g) and 0.8 (h). Negative vorticity is represented in bold lines and positive vorticity in simple lines. The relative vorticity extremum is $\omega/\omega_{\text{ref}} = \pm 4$ and the contour intervals are 0.4.

flow, obtained from measurements realised in the upstream and downstream visualisation zones, for three different phases ($t/T = 0, 0.32, 0.68$). Thus, the plots of Fig. 5(a), (e), (g) and Fig. 6(a)–(c) correspond to two different measurements at different resolutions, but at the same phases (*i.e.* $t/T = 0, 0.32, 0.68$). Bold lines correspond to negative and simple lines to positive vorticity; the time is dimensionless.

Downstream of the plate, the boundary layer detaches at the edge due to the velocity shear. It then rolls up around and above the plate, leading to the formation of a negative sign vortex (Fig. 5(a)). The formation of this vortex creates a boundary layer of positive vorticity between the vortex and the plate (Fig. 5(b), (c)), which then detaches leading to a positive shear layer when the negative vortex is advected downstream by the mean flow (Fig. 5(d), (e)). This shear layer is reinforced by a strong velocity gradient between the upper and lower plate flows (Fig. 5(f), (g)).

While the negative vortex is formed at the lee-side edge (Fig. 5(a)–(e)), the positive shear layer formed at the previous wave period is destabilised and leads to the formation of a positive sign vortex (Fig. 6(a), (b)). The instantaneous streamline fields on the lee-side zoomed view show wavy structures (not shown here) with a wavelength about $\lambda = 6.2$ mm and a shear layer thickness estimated at $\delta = 0.4$ mm close to the plate. The dimensionless wavenumber is then $k = 2\pi\,\delta/\lambda = 0.4$ and seems to correspond to the most unstable wavenumber of the Kelvin Helmotz instability [32]. However, this supposition needs to be further supported by other studies for varying parameters (wave period T, plate length L, immersion i, etc.) in order to be confirmed. Once the positive vortex is formed, the counter rotating vortex pair is advected toward the bottom due to mutual induction (Fig. 6(b)). During that time, these vortices undergo 3D instabilities, which eventually lead to their breakdown.

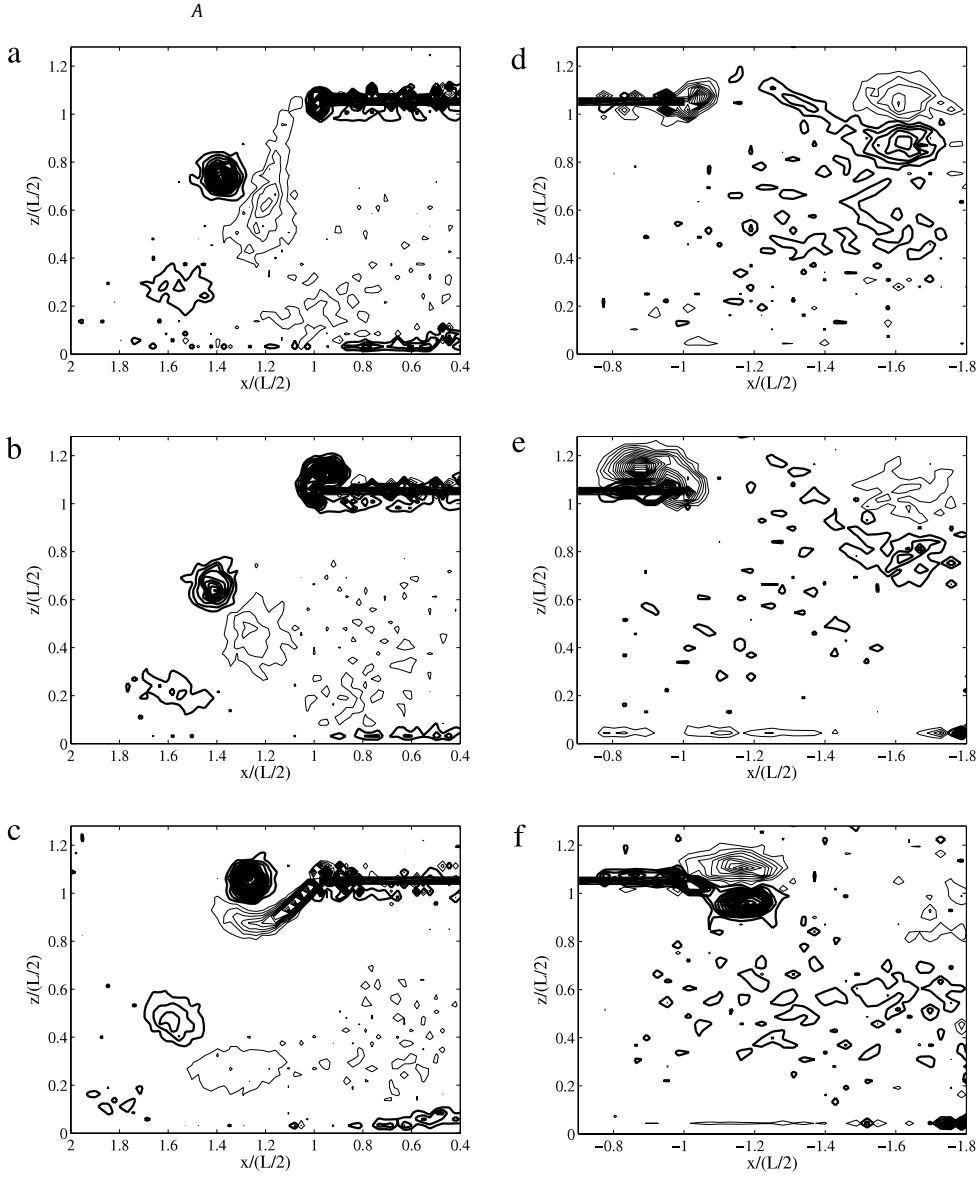

Fig. 6. Mean vorticity fields downstream the plate (left panel) and upstream (right panel) at $t/T = 0$ (a,d), 0.32 (b,e) and 0.68 (c,f). Negative vorticity is represented in bold lines and positive vorticity in simple lines. The relative vorticity extremum is $\omega/\omega_{\text{ref}} = \pm 0.8$ and the contour intervals are 0.04.

Upstream of the plate, a positive vortex is formed, first due to flow separation. One half period later, a second vortex of opposite sign vorticity is generated. Both are advected upstream in a quasi-horizontal direction since they have similar intensity when shed from the plate. During the following wave period, they remain at nearly the same location from where they are dissipated.

Fig. 7 shows the upstream and downstream vortex trajectories over two wave periods. The vortex core positions can be determined till $t/T \approx 1.3$ upstream and $t/T \approx 1.9$ downstream. After those times, the vortex centres cannot be detected anymore owing to the previously described breakdown and dissipation process. However, residual vorticity remains in the flow (Fig. 6(c), (f)). The trajectory of the positive downstream vortex presents discontinuities since its formation is very rapid and hard to follow with the present spatial and temporal resolutions. Due to mutual induction, both upstream and downstream vortex pairs are advected from the plate edges at a distance of about 1/3 the plate length. However, upstream vortices are advected horizontally whereas downstream vortices are advected toward the bottom, over a distance approximately equal to 1/6 of the total water depth but nearly 3/4 of the immersion *i*. This strong downward movement may lead to strong stresses and perturbations of the seabed.

The strong asymmetry observed in the behaviour of upstream and downstream vortex pairs is due to a global convection induced by the wave flow and its interaction with the plate. Indeed, the wave propagation induces an asymmetric flow between the crest and the trough of the waves. Moreover, the shallow-water flow above the plate increases this asymmetry.

This asymmetry is confirmed by the measurement of the circulation around the plate over one period (Fig. 8). This circulation is compared with the circulation calculated using the analytical model [8,10,12]. In this model the instantaneous circulation is non zero due to velocity discontinuities at the edges of the plate. Thus, the plate circulation has a periodic oscillation both for the potential flow theory and the experiments. This periodic oscillation of the plate circulation gives an indication of the hydraulic forces affecting the plate over one wave period. However, in the experiments the maximum value of the circulation is about three times higher than the one calculated with the potential flow theory. On top of that, the mean circulation over one period is non zero $\bar{\Gamma}/(2LU) = 0.086$ whereas it is zero for the potential flow solution. This mean circulation may be partly explained by the measurement method, *i.e.* integrating the velocity on the closest rectangular contour around the plate on the global

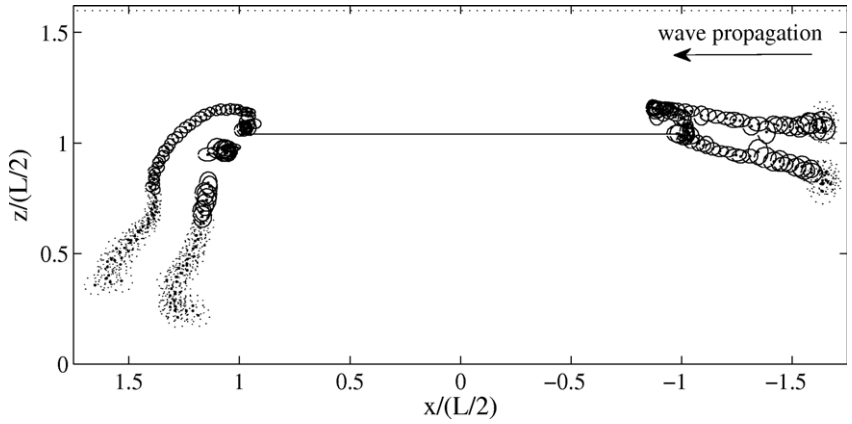

Fig. 7. Vortex trajectories over two wave periods. The dots represent the mean position of the vortices, the solid (resp. dotted) lines represent the standard deviation computed for the 300 periods for each position during the first (resp. second) wave period.

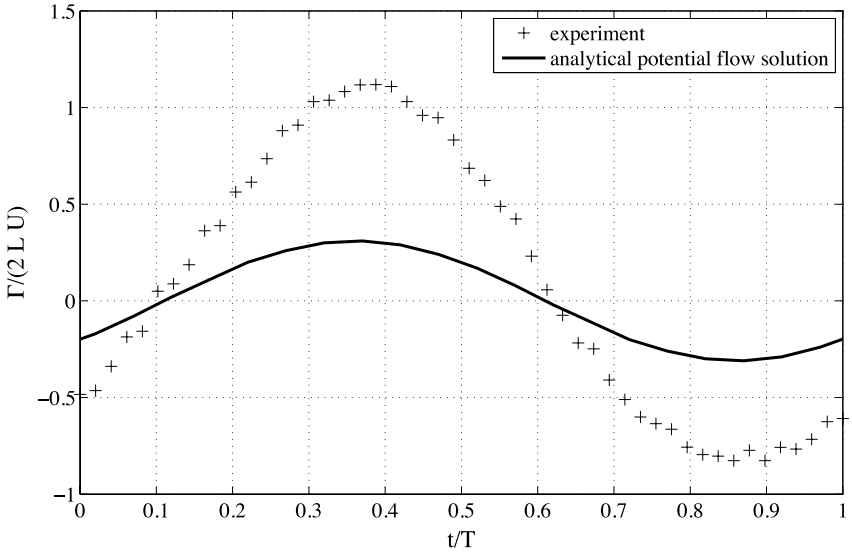

Fig. 8. Evolution of the dimensionless circulation around the plate over one wave period calculated from the experiments (+) and the potential flow theory (−).

view field. Since the resolution is rather rough on the global view, one cannot remove the velocities generated by the vortices at the plate edges. However, the measurement method cannot explain all the differences between the experimental and the theoretical circulation. Indeed, the discrepancies may also be explained by the fact that the theoretical model is linear whereas the free surface is nonlinear above the plate due to the shallow water depth. This has two consequences: phase-locked and free harmonics are generated [26] and the velocity profile above the plate tends to be uniform, leading to higher velocities close to the plate than those predicted by the theory. Moreover, the large recirculation cells present under the plate are not reproduced by the potential flow theory. Thus, the non-zero mean circulation and the asymmetry of the experimental curve has a physical meaning explained by the asymmetry of the wave flow.

Fig. 9 shows the evolution of the vortices' circulation over two periods. The circulation is computed as the vorticity integral on a surface delimited by the distance from the vortex centre at which the vorticity value is one sixth of its local extremum. Although this threshold seems arbitrary, changing the way the circulation is computed did not change the circulation evolution.

Three development phases are observable for the positive upstream vortex: a growth phase, a strong decrease phase and a dissipation phase. During the phase of vortex formation above the plate, the circulation strongly increases between $t/T = 0$ and $t/T \approx 0.2$. Then, the circulation strongly decreases while the vortex remains above the plate, between $t/T \approx 0.2$ and $t/T \approx 0.6$. As soon as the vortex detaches from the edge of the plate, the circulation decreases again with a power law about $t^{-0.7}$. Three development phases are also observable for the negative downstream vortex: a stagnation phase, a growth phase and a dissipation phase. During the stagnation phase, the vortex remains above the plate. The circulation is then more or less constant between $t/T = 0$ and $t/T \approx 0.4$. Then, the circulation increases from $t/T \approx 0.4$ to $t/T \approx 0.7$. For times larger than $t/T \approx 0.7$, the circulation decreases with a power law about $t^{-0.8}$. The evolution of the downstream positive vortex and upstream negative vortex are different as they form later on. Their circulation increases during a phase of formation and a quarter of a period later they dissipate with a power law about $t^{-0.6}$ and $t^{-0.7}$. This dissipation is linked to three dimensional instabilities under study. The vortex filaments are then strongly deformed and burst. The destruction of vortices occurs earlier for the upstream vortices ($t/T \approx 1.26$) than for the downstream ones ($t/T \approx 1.86$).

5. Conclusion

The 2D dynamics of the flow around a submerged plate for a given wave condition has been presented and characterised. This experimental study has been carried out using PIV measurements.

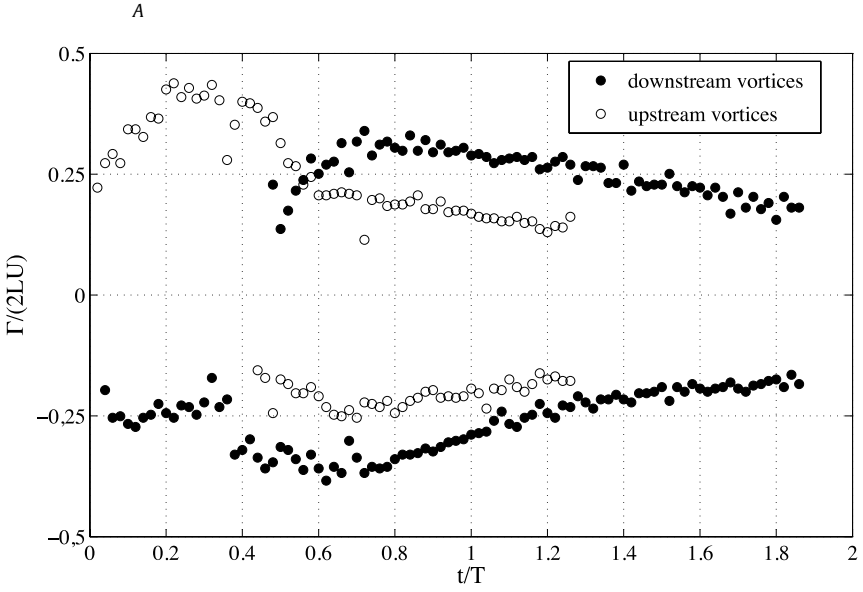

Fig. 9. Evolution of the dimensionless circulation for the upstream and downstream vortices over two wave periods.

Vortices are periodically generated and shed at the weather and lee-side edges of the plate. Those vortices considerably modify the mean flow and, as a matter of consequence, vortices cannot be neglected when considering the local flow around a submerged structure. In the present case, two counter rotating recirculation cells are formed under the plate leading to two stagnation points at the flume bottom. These stagnation points could lead to scouring or accumulation phenomena, when considering a sedimentary bed. At the upstream (resp. downstream) plate edge, a positive (resp. negative) vortex is formed by shedding and curling up the plate boundary layer. About one half period later, opposite sign vortices are generated and both vortex pairs are advected due to mutual induction over nearly two periods, leading to strong velocities. These velocities can reach up to three times the characteristic velocity U. The downstream vortex pair leads to a strong jet, which impacts the flume bottom, whereas upstream of the plate, positive and negative vortices are advected horizontally in front of the obstacle and do not interact with the bottom. During their advection, vortices are deformed and distorted through three dimensional instabilities, which eventually lead to their dissipation. The detailed characterisation of those instabilities thanks to stereo photography is under consideration.

However, the presented dynamics are completely different from those predicted by potential theories. The behaviour of the vortices has to be considered to analyse the impacts of any immersed structure, when considering scouring of the sedimentary bed, loading on the structure itself or neighbouring structures. Despite the simple geometry considered in this study, many parameters might be of importance, among which the plate length over wavelength ratio, the immersion over water depth ratio, wave frequency or wave amplitude. To study the influence of those parameters on vortex dynamics, and determine which are the most relevant ones, a full parametric analysis is required. Considering the total number of parameters, a numerical modelling would be more appropriate. A 2D numerical model has been developed in a Lagrangian frame using Vortex Method in a velocity–vorticity formulation. This model is under validation using the present experimental study. The numerical results and the parametric analysis will be presented in the second part of this paper.

Acknowledgment

This work was supported by Région Haute-Normandie.

References

[1] J.A. Liggett, Fluid Mechanics, McGraw-Hill, 1994.
[2] K.A. Chang, T.J. Hsu, P.L.F. Liu, Vortex generation and evolution in water waves propagating over a submerged rectangular obstacle. Part I: solitary waves, Coastal Eng. 44 (2001) 13–36.
[3] M. Brocchini, D.H. Peregrine, The dynamics of strong turbulence at free surfaces. Part I description, J. Fluid Mech. 449 (2001) 225–254.
[4] B.M. Sumer, R.J.S. Whitehouse, A. Torum, Scour around coastal structures: a summary of recent research, Coastal Eng. 44 (2001) 153–190.
[5] D.M. Young, F.Y. Testik, Onshore scour characteristics around submerged vertical and semicircular breakwaters, Coastal Eng. 56 (2009) 868–875.
[6] F.C.K. Ting, Y.K. King, Vortex generation in water waves propagating over a submerged obstacle, Coastal Eng. 24 (1994) 23–49.
[7] K.A. Chang, T.J. Hsu, P.L.F. Liu, Vortex generation and evolution in water waves propagating over a submerged rectangular obstacle. Part II: Cnoidal waves, Coastal Eng. 52 (2005) 257–283.
[8] K. Takano, Effets d'un obstacle parallélépipédique sur la propagation de la houle, Houille Blanche 15 (1960) 247–267.
[9] P.F. Siew, D.G. Hurley, Long surface waves incident on a submerged horizontal plate, J. Fluid Mech. 83 (1) (1977) 141–151.
[10] S.R. Massel, Harmonic generation by waves propagating over a submerged step, Coastal Eng. 7 (1983) 357–380.
[11] M. Patarapanich, Maximum and zero reflection from submerged plate, J. Waterw. Port Coast. Ocean Eng.-ASCE 110 (2) (1984) 171–181.
[12] V. Rey, M. Belzons, E. Guazzelli, Propagation of surface gravity waves over a rectangular submerged bar, J. Fluid Mech. 235 (1992) 453–479.
[13] R. Usha, T. Gayathri, Wave motion over a twin-plate breakwater, Ocean Eng. 32 (2005) 1054–1072.
[14] S. Neelamani, T. Gayathri, Wave interaction with twin plate wave barrier, Ocean Eng. 33 (2006) 495–516.
[15] K.U. Graw, Shore protection and electricity by submerged plate wave energy converter, in: European Wave Energy Symposium, 1993, pp. 1–6.
[16] K.U. Graw, The submerged plate wave energy converter. a new type of wave energy device, in: ODEC, 1993, pp. 1–4.
[17] R.W. Carter, Wave energy converters and submerged horizontal plate, Ph.D. Thesis, Thesis of University of Hawaii, 2005.
[18] G. Orer, A. Ozdamar, An experimental study on the efficiency of the submerged plate wave energy converter, Renew. Energy 32 (2007) 1317–1327.
[19] J. Lengricht, K.U. Graw, H. Kronewetter, Stereoscopic PIV adapted to gravity wave analysis, in: 10th International Symposium on Applications of Laser Techniques to Fluid Mechanics, 2000.
[20] T. Whittaker, D. Collier, M. Folley, M. Osterried, A. Henry, M. Crowley, The development of Oyster—a shallow water surging wave energy converter, in: 7th European Wave Tidal Energy Conference, Porto, Portugal, 2007.
[21] M. Folley, T. Whittaker, J. van't Hoff, The design of small seabed-mounted bottom-hinged wave energy converters, in: 7th European Wave and Tidal Energy Conference, Porto, Portugal, 2007.
[22] A.F. de O. Falcão, Wave energy utilization: a review of the technologies, Renew. Sustainable Energy Rev. 14 (3) (2010) 899–918.
[23] O.L. Maître, S. Huberson, E.S.D. Cursi, Unsteady model of sail and flow interaction, J. Fluid Struct. 13 (1999) 37–59.
[24] J.N. Newman, Marine Hydrodynamics, MIT Press, 1977.

[25] Y. Goda, Y. Suzuki, Estimation on incident and reflected waves in random wave experiments, in: 15th Coastal Engineering Conference, 1976, pp. 828–845.
[26] J. Brossard, G. Perret, L. Blonce, A. Diedhiou, Higher harmonics induced by a submerged horizontal plate and a submerged rectangular step in a wave flume, Coastal Eng. 56 (1) (2009) 11–22.
[27] G.K. Batchelor, Introduction to Fluid Dynamics, Cambridge University Press, 1967.
[28] J. Hunt, A. Wray, P. Moin, Eddies, streams, and convergence zones in turbulent flows, in: Studying Turbulence Using Numerical Simulation Databases, vol. 2, 1988, pp. 193–208.
[29] M.S. Chong, A.E. Perry, B.J. Cantwell, A general classification of three-dimensional flow-fields, Phys. Fluids 2 (5) (1990) 765–777.
[30] J. Jeong, F. Hussain, On the identification of a vortex, J. Fluid Mech. 285 (1995) 69–94.
[31] L. Graftieaux, M. Michard, N. Grosjean, Combining PIV, POD and vortex identification algorithms for the study of unsteady turbulent swirling flows, in: Euromech Colloquium on 3C Stereo and Holographic PIV, Measurement Science and Technology, vol. 12(9), 2001, pp. 1422–1429.
[32] F. Charru, Instabilités Hydrodynamiques, CNRS Editions, Paris, 2007, Savoirs, Actuels.